

Covering factors of the dusty obscurers in radio-loud and radio-quiet quasars

Maitrayee Gupta[★], Marek Sikora[†], Krzysztof Nalewajko[‡]

Nicolaus Copernicus Astronomical Center, Bartycka 18, 00-716 Warsaw, Poland

Last updated 2016 March 11; in original form 2016 March 11

ABSTRACT

We compare covering factors of circumnuclear dusty obscurers in radio-loud and radio-quiet quasars. The radio-loud quasars are represented by a sample of FR II quasars obtained by cross-matching a catalog of the FR II radio sources selected by van Velzen et al. with the SDSS DR7 catalog of quasars. Covering factors of FR II quasars are compared with covering factors of the radio-quiet quasars matched with them in redshift, black hole mass, and Eddington-ratio. We found that covering factors, proxied by the infrared-to-bolometric luminosity ratio, are on average slightly smaller in FR II quasars than in radio-quiet quasars, however, this difference is statistically significant only for the highest Eddington ratios. For both samples, no statistically significant dependence of a median covering factor on Eddington ratio, black hole mass, nor redshift can be claimed.

Key words: quasars: general – infrared: galaxies

1 INTRODUCTION

Discovery of broad lines and strong non-stellar continuum in polarized light of Seyfert 2 galaxies (Antonucci & Miller 1985; Miller & Goodrich 1987) and thermal infrared (IR) excesses (Miley et al. 1985; Edelson et al. 1987) led to idea about existence in active galactic nuclei (AGN) of dusty, molecular tori (Krolik & Begelman 1988). This allowed us to unify Seyfert 2 galaxies (only narrow lines and weak or absent non-stellar continuum) with Seyfert 1 galaxies (broad emission lines and strong non-stellar continuum). The dusty tori were proposed also to unify narrow-line radio galaxies with radio-loud (RL) quasars and broad-line radio galaxies (Barthel 1989), and discovery of radio-quiet (RQ) quasars of type 2 (Reyes et al. 2008 and refs. therein) confirmed the presence of dusty obscurers in RQ quasars as well.

As indicated by the number ratio of the type 2 AGN to the type 1 AGN, and, independently, by the infrared-to-UV luminosity ratio, these tori are geometrically thick (Netzer 2015). They are predicted to have inner edge at the sublimation radius (Rees et al. 1969; Barvainis 1987) and are likely enclosed within the black hole (BH) influence sphere (Hopkins et al. 2012 and refs. therein). Location of the inner edge at the sublimation radius is confirmed by reverberation mappings (e.g. Koshida et al. 2014) and by near-IR interferometry (Kishimoto et al. 2012), while constraints on their spatial extensions are suggested by the mid-IR interferometry (Bartscher et al. 2013; López-Gonzaga et al. 2016). Hence, studies of such tori provide excellent opportunity to probe the conditions

of the outermost portions of the BH accretion flows. Unfortunately, physical and dynamical structure of dusty tori is still not known (see review by Netzer 2015). It is even uncertain, whether they are really tori, or maybe the tori are just mimicked by optically thick portions of disc winds (e.g. Emmering et al. 1992; Königl & Kartje 1994; Elitzur & Shlosman 2006) or by warped, tilted accretion discs (Lawrence & Elvis 2010 and refs. therein). One might try to resolve the real structure of the dusty region by modelling spectra of IR radiation resulting from reprocessing of optical/UV central radiation (see e.g. Stalevski et al. 2016). However, due to the complexity of these models, the observed spectra can be reproduced by many of them with a broad choice of the adopted model parameters (Netzer et al. 2016).

Regardless of the uncertainties in the ‘torus’ structure, using the mid-IR spectra one can at least study the fraction of the central radiation that is reprocessed by circumnuclear dust ($R \equiv L_{\text{MIR}}/L_{\text{bol}}$), in particular its distribution and dependence on the Eddington ratio ($\lambda_E \equiv L_{\text{bol}}/L_{\text{Edd}}$) and black hole mass (M_{BH}). Noting that luminous RQ and RL quasars cover similar ranges of these parameters, by comparing above properties in these two quasar populations one may try to verify whether the conditions in their outer accretion discs are different, as one might expect in case of having accretion triggered by mergers in RL quasars and by secular processes in RQ quasars (Chiaberge et al. 2015), and/or having accretion flows characterized by higher magnetization in the RL quasars as compared with the RQ ones. Obviously, if existing, the largest difference in the R should be noticed between the RQ quasars and the most RL ones. Hence, unlike in similar studies performed by Ma & Wang (2013), our RL quasar sample was chosen to be represented only by quasars with Fanaroff-Riley Class II (FR II) radio-morphology. Furthermore, in order to exclude possible differenti-

[★] E-mail: mgupta@camk.edu.pl

[†] E-mail: sikora@camk.edu.pl

[‡] E-mail: knalew@camk.edu.pl

ating effects coming from different BH masses, Eddington-ratios, and redshifts, we perform such comparison by respective pairings of RL and RQ quasars. First, when deriving dependence of R on λ_E , we pair each RL quasar with a RQ one with the same redshift and black hole masses. Secondly, when studying dependence of R on the black hole mass, we pair quasars with the same redshift and λ_E . Thirdly, when studying dependence of R on the redshift, we pair quasars with the same λ_E and black hole mass.

Our work is organized as follows: in §2 we define our data samples, in §3 the methods of calculation of R and pairing procedures are described, in §4 results of our studies of covering factors of dusty obscurers in FR II versus RQ quasars are presented, and in §5 they are discussed in the context of the radio diversity of quasars. We adopted Λ cold dark matter cosmology, with $H_0 = 70 \text{ km s}^{-1}$, $\Omega_m = 0.3$ and $\Omega_\Lambda = 0.7$.

2 DATA SAMPLES

2.1 FR II quasars

A large catalogue of 59192 FR II radio sources (Fanaroff & Riley 1974) was recently compiled by van Velzen et al. (2015), using data from the Faint Images of the Radio Sky at Twenty-centimetres (FIRST) catalogue (Becker et al. 1995). From this, van Velzen et al. (2015) selected a sample of 1108 FR II quasars by matching their FR II radio sources with the combined DR7 and DR9 catalogues of SDSS quasars. We are interested only in the DR7 quasars, for which black hole mass estimates are available (Shen et al. 2011). Since sources that are both in the DR7 and DR9 are denoted as ‘DR9’, in order to select all DR7 quasars, we performed additional matching of the FR II quasar sample of van Velzen et al. (2015) (1108 sources) with the SDSS DR7 quasar catalogue (Schneider et al. 2010) (105783 sources). We used a matching radius of 5 arcsec and obtained 899 objects. This resulting sample of FR II quasars was then matched with the sample of SDSS DR7 quasars detected by the *Wide-field Infrared Survey Explorer* (WISE) (Wu et al. 2012). This gave us 895 FR II quasars detected in the MIR band.

2.2 Radio-quiet quasars

The RQ sample with MIR data is constructed by matching the DR7 quasar catalogue (Schneider et al. 2010) and WISE all-sky catalogue (Wu et al. 2012), using a matching radius of 1 arcsec, resulting in 101853 objects. From these we remove the 899 RL quasars matched with the catalog by van Velzen et al. (2015), this leaves us with 100958 quasars. We then remove objects that were detected by the FIRST survey (Becker et al. 1995), this gives us 92648. We repeat the same process with the NVSS (Condon et al. 1998) and end up with 92445 objects. We also removed those objects that were outside the FIRST observation region.

2.3 Additional sample criteria

As it is stated in §3, we calculate the MID infrared luminosity, using the flux measured in the WISE/W3 window ($\lambda \approx 12 \mu\text{m}$). In order to avoid having this window too close to the short-wavelength edge of the MIR band in the quasar rest frame, we limit our samples to $z < 2$. We also introduce a limit on black hole masses, taking only quasars with $M_{\text{BH}} > 10^8 M_\odot$. This is in order to avoid Seyfert galaxies, in which the MIR flux can have a significant contribution from

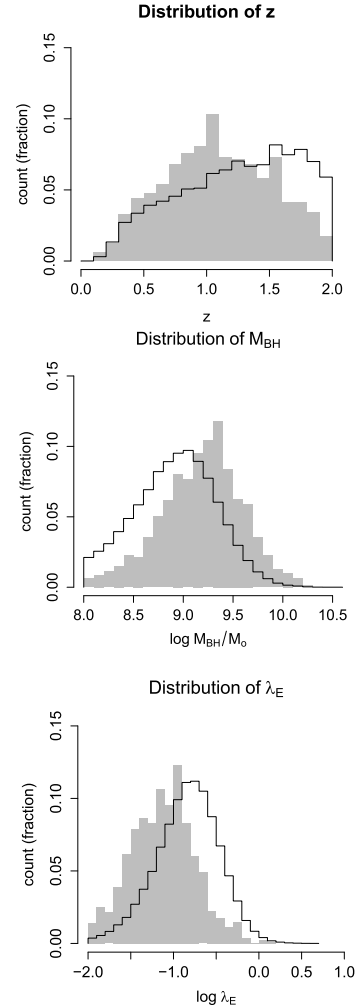


Figure 1. Distributions of our RL (grey) and RQ (unfilled) samples of quasars in redshift z , black hole mass M_{BH}/M_\odot , and Eddington ratio $\lambda_E = L_{\text{bol}}/L_{\text{Edd}}$.

starbursts. Furthermore, putting limits on redshift and black hole mass reduces biases imposed on studied properties by selection effects related to the flux limits. Finally, we constrain our samples to the objects with the Eddington-ratio $\lambda_E > 0.01$ to assure that accretion flows in the selected objects are radiatively efficient. After applying all these limits we end-up with 797 FR II quasars and 67480 RQ quasars.

In Figure 1 we show the histograms of our RL and RQ samples as a function of redshift z , black hole mass M_{BH}/M_\odot , and Eddington ratio λ_E .

3 METHODS

3.1 Covering factor

There are two main methods to derive covering factors of dusty, circumnuclear obscurers, using number ratio of type 1 to type 2 AGNs or using ratio of the MIR luminosity to the bolometric luminosity (see review by Netzer 2015). Both methods suffer from several drawbacks, the former because of difficulties to assure the common parent AGN population and because of having dependence of N_2/N_1 on the covering factor distributions (Ramos Almeida et al.

Table 1. Center wavelengths and frequencies of the four WISE bands. The fourth column gives Δm which is used to transform the the given Vega magnitudes to the AB magnitude system.

Band	$\lambda(\mu\text{m})$	$\log(\nu)$ (Hz)	Δm
1	3.435	13.94	2.699
2	4.6	13.81	3.339
3	11.56	13.41	5.174
4	22.08	13.13	6.620

2011; Elitzur 2012), the latter because derivation of the covering factor from $L_{\text{MIR}}/L_{\text{bol}}$ requires knowledge of anisotropy of accretion disc and obscurer radiation, and those are model dependent. In this paper we will assume that the covering factor is simply equal to $R \equiv L_{\text{MIR}}/L_{\text{bol}}$, which corresponds with the assumption of isotropic radiation of both components. While quantitatively this may lead to large systematic departures from real values of covering factors (see, e.g. Calderone et al. 2012), as long as our main interest is to verify whether dusty obscurers in RL and RQ quasars are different, using R is not expected to affect trends studied by us. We calculate R taking L_{bol} from Shen et al. (2011) and L_{MIR} using formula $L_{\text{MIR}} = 12.5 \times (\nu_{\text{W3}} L_{\nu, \text{W3}})$, where $\nu_{\text{W3}} = 10^{13.4}$ Hz, $L_{\nu, \text{W3}} = 4\pi d_L^2 F_{\nu, \text{W3}}$, $\log F_{\nu, \text{W3}} = -(5.174 + m_{\text{W3}})/2.5$, and m_{W3} magnitudes are provided by Wu et al. (2012), denoted in Table 1 as ‘W3’.

Our choice of using WISE/W3 data to calculate L_{MIR} can be justified by noting that:

- circumnuclear dust spectra in the AGN rest frames are approximately flat, i.e., with a spectral index $\alpha_{\text{MIR}} \approx 1$ ($\alpha : F_\nu \propto \nu^{-\alpha_{\text{MIR}}}$) and enclosed between $2\mu\text{m}$ and $25\mu\text{m}$ (Hönig et al. 2011; Netzer 2015);
- for redshifts $z > 1.3$ the W1 and W2 bands move in the quasar rest frame to $\lambda_E < 2\mu\text{m}$;
- W4 fluxes have much larger S/N than in other channels, hence calculating L_{MIR} by using spectral slopes between separated by less than factor of 2 ν_{W2} and ν_{W3} may create much larger errors than using only W3 flux and adopting $\alpha_{\text{MIR}} = 1$.

3.2 Pair Matching

We use a matching technique used in Kauffmann et al. (2008), Masters et al. (2010) and Wild et al. (2010) instead of globally comparing the properties of the RL and RQ samples with different distributions of black hole mass or redshift. In order to study the dependence of R on any of the three parameters λ_E , M_{BH} or z , each RL quasar is associated with the same number n of RQ quasars according to their matching distance calculated for the other two parameters. First, candidate RQ counterparts are selected from the following range: $|\Delta \log \lambda_E| < 0.09$, $|\Delta z| < 0.01$ and $|\Delta \log M_{\text{BH}}| < 0.12$. Secondly, we calculate the matching distances between the RL quasar and the RQ candidates defined as $d_{\text{match}}^2 = \sum_i \Delta_i^2$, where Δ_i stands for either $\Delta \log \lambda_E$, Δz or $\Delta \log(M_{\text{BH}}/M_\odot)$. Then, we select only those RQ candidates which have the shortest matching distance d_{match} . We have considered different numbers of paired RQ quasars with $n = 1, 3, 10$. This process of matching can result in the same RQ quasar paired with more than one RL ones.

Then, the sample of RL quasars, and the subsample of paired RQ quasars, are divided according to the studied parameter into several bins containing equal number of sources. For example, in

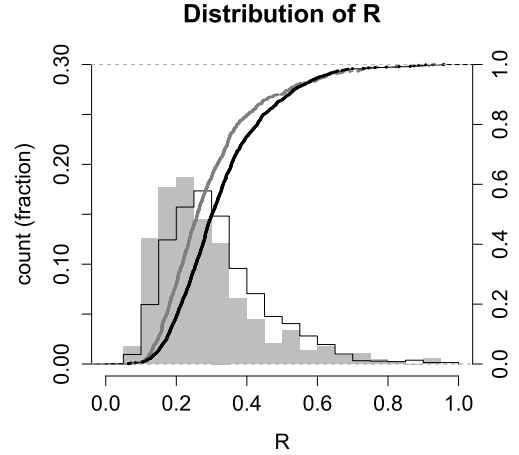


Figure 2. Normalised and cumulative distributions of dust covering factor R for our RL sample (grey) and the RQ subsample paired with $n = 3$ (unfilled / black).

order to study the dependence of R on λ_E , we divide the samples in the bins of λ_E , and then we pair the quasars in M_{BH} and z according to the matching distance given by $d_{\text{match}}^2 = (\Delta z)^2 + [\Delta \log(M_{\text{BH}}/M_\odot)]^2$.

4 RESULTS

Figure 2 compares the overall normalized distributions of R for RL and RQ quasars that are paired in z , M_{BH} and λ_E with $n = 3$. We have overlaid the cumulative distributions of the two samples. The typical values of R for both RL and RQ quasars are in the range 0.1 – 0.6. The histograms peak at $R_{\text{peak}} \approx 0.25$, with R_{peak} being slightly higher for the RQ quasars. The mean values of R are 0.28 for RQ quasars and 0.32 for RL quasars, and the median values are 0.25 and 0.29, respectively.

In Figure 3 and Figure 4 we show the distributions of R versus either λ_E , M_{BH} or z for the paired samples of RL and RQ quasars.

Table 2 reports the median values R_{50} , as well as first and third quartiles R_{25} and R_{75} for different bins of λ_E , corresponding to the left panel of Figure 3. There is no overall trend that we see in the distribution of R . The difference in R between RL and RQ increases with the increase in λ_E , z , and M_{BH} . This trend remains the same, irrespective of the number of matches being $n = 1, 3, 10$, and whether the bins are equally spaced or contain equal number of objects. We added an additional plot Figure 5 with equal sized wide bins and we do not see any changes in the trend.

We also observe that R_{25} and R_{75} indicate broad distributions of R for every λ_E , M_{BH} and z . Therefore, variations in the median values do not appear to be significant.

Figure 6 shows the cumulative distributions of R for the samples shown in Figure 3 divided according to λ_E into bins containing equal number of objects. In order to evaluate whether there are statistical differences between the distributions of R for RL and RQ samples, we make use of the two-sample Kolmogorov-Smirnov test (K-S test). Table 3 shows the D -values and p -values of each bin. For a broad range of λ_E values, the values of p range between 0.001 and 0.15, indicating that the difference between the distributions of R are not very significant.

However, for the highest values of $\log \lambda_E \in [-0.69 : 0.11]$, we obtain $p < 10^{-9}$, which indicates significant discrepancy, with the RL quasars having median covering factors lower by $\Delta R = 0.094$.

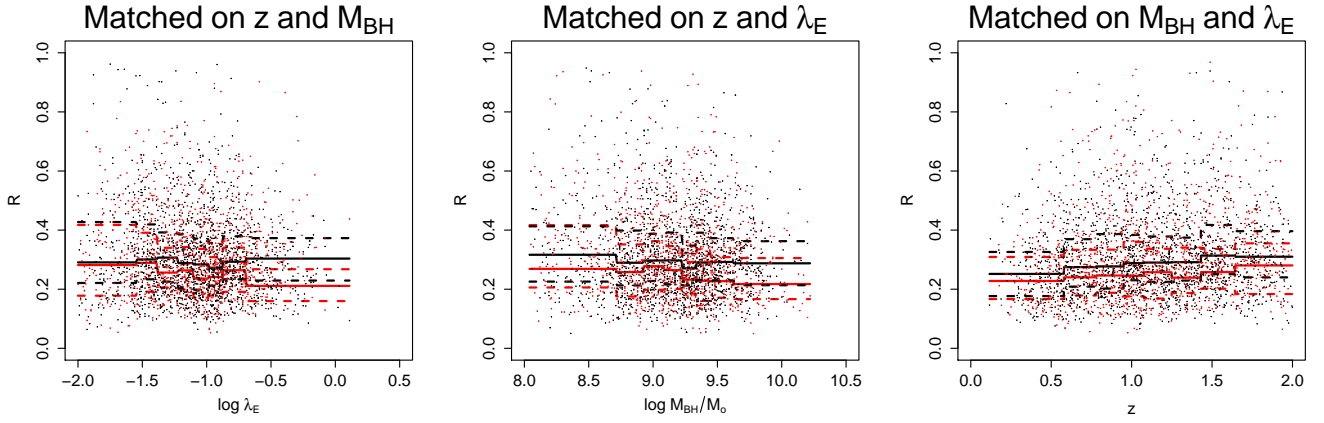


Figure 3. Dependence of R on Eddington ratio λ_E shown in the *left panel*, black hole mass M_{BH} shown in the *middle panel* and redshift z as shown in the *panel to the right*. The *red points* represent the RL sample, while *black points* represent the RQ subsample paired with $n = 3$. The *solid lines* show the median value for bins containing equal numbers of sources. The *dashed lines* represent the 25th and 75th percentiles of the respective data.

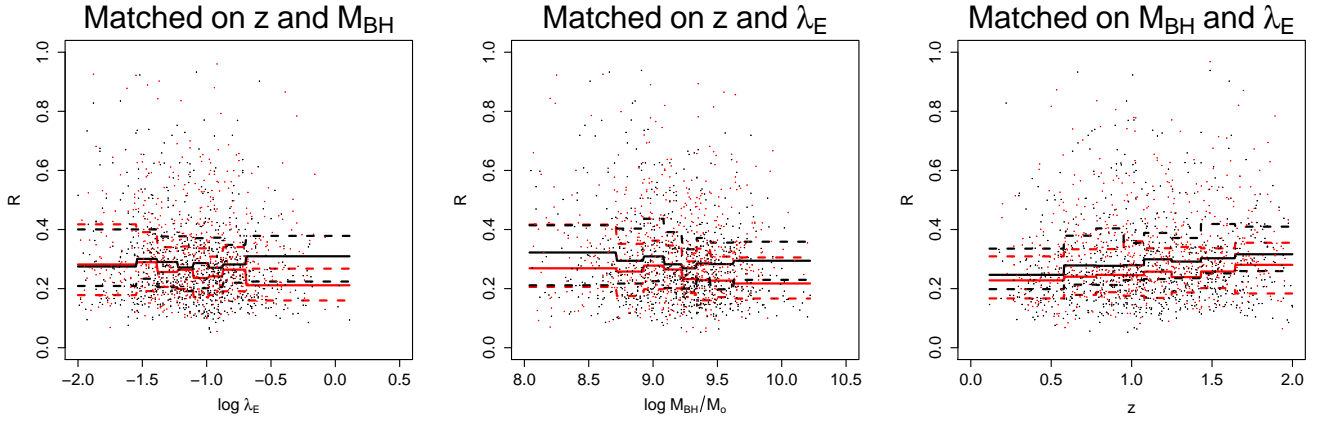


Figure 4. Same as Figure 3, but for $n = 1$.

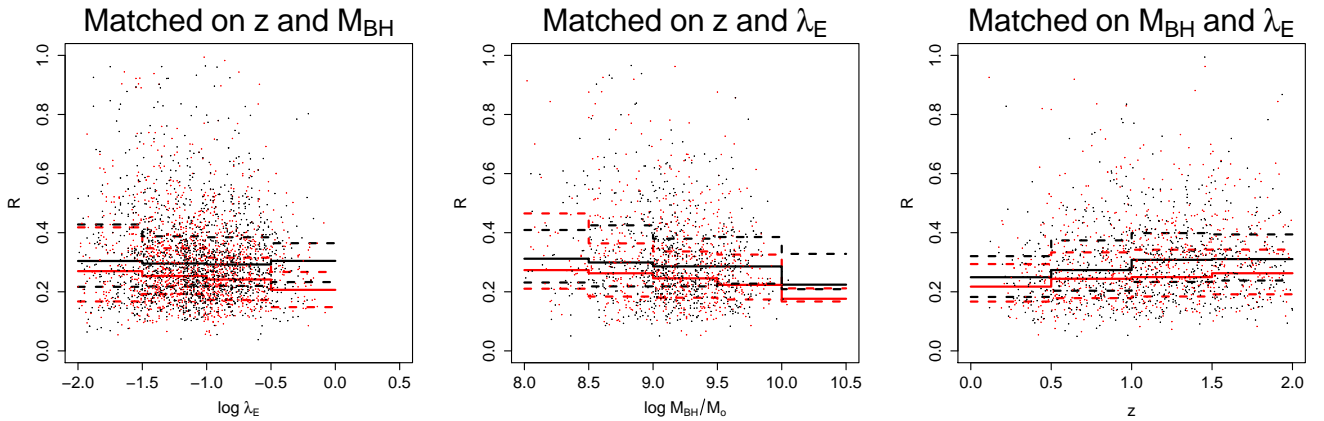


Figure 5. Same as Figure 3, but with equal sized bins.

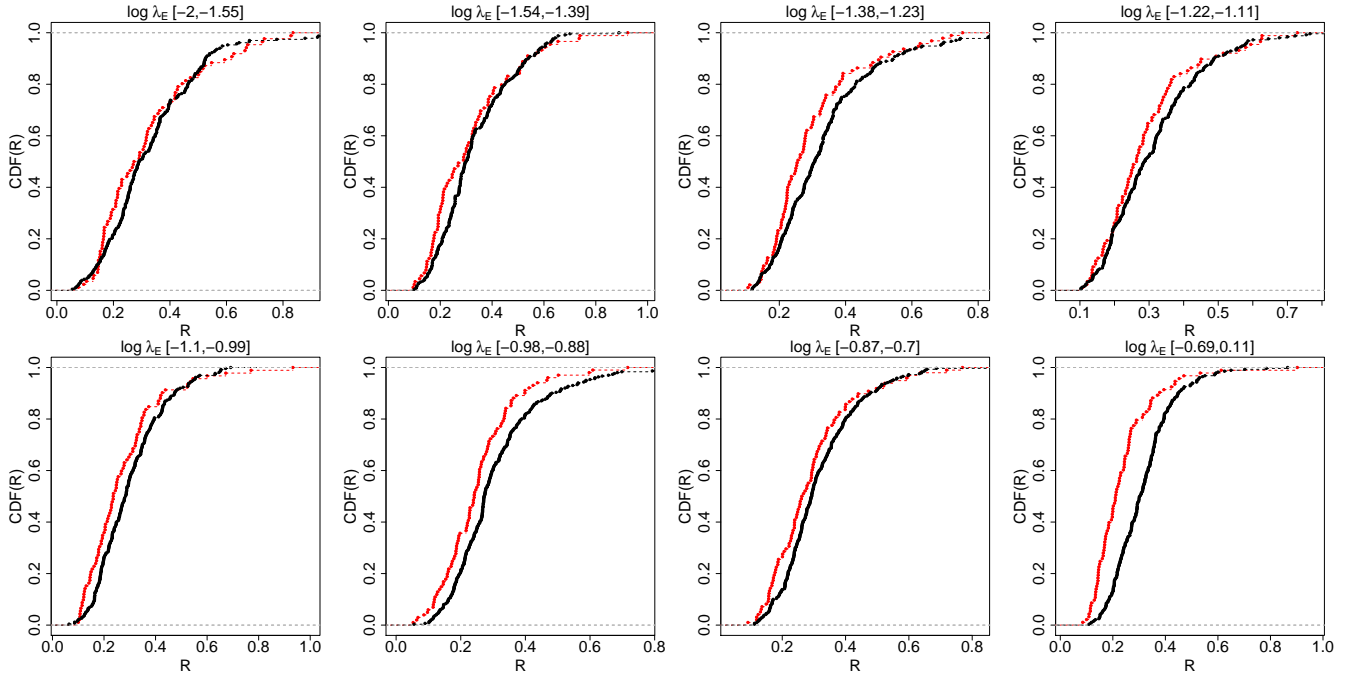


Figure 6. Cumulative distributions of R for the subsamples of RL quasars (red) and RQ quasars (black) paired with $n = 3$ for several bins of the Eddington ratio λ_E containing equal number of sources.

Table 2. Tabulated results of the sample matched on z and M_{BH} . We show the median value of λ_E for each of the bins, the numbers of sources N , the median value of R , the standard deviation of R distribution σ_R , and the 25th and 75th percentiles of R .

$\log \lambda_{E,50}$	class	N	R_{50}	σ_R	R_{25}	R_{75}
-1.695	RL	86	0.282	0.177	0.178	0.418
-1.71	RQ	233	0.291	0.170	0.221	0.427
-1.45	RL	89	0.289	0.164	0.192	0.391
-1.46	RQ	249	0.301	0.142	0.234	0.419
-1.31	RL	95	0.256	0.140	0.206	0.340
-1.3	RQ	271	0.307	0.155	0.226	0.392
-1.17	RL	88	0.264	0.132	0.199	0.343
-1.15	RQ	253	0.288	0.136	0.204	0.385
-1.04	RL	92	0.236	0.148	0.171	0.336
-1.04	RQ	261	0.284	0.127	0.198	0.371
-0.93	RL	101	0.242	0.116	0.178	0.308
-0.93	RQ	301	0.273	0.143	0.212	0.357
-0.8	RL	98	0.264	0.131	0.191	0.341
-0.79	RQ	290	0.293	0.121	0.234	0.379
-0.54	RL	93	0.211	0.122	0.160	0.268
-0.53	RQ	282	0.304	0.114	0.229	0.373

5 DISCUSSION AND CONCLUSIONS

While the main factor determining the radiative efficiency of accretion flows in AGN is the accretion rate normalized by the black hole mass (equivalently, the accretion-rate Eddington ratio $\dot{M}c^2/L_E$), the efficiency of jet production covers 3–4 orders of magnitude at any Eddington ratio (Sikora et al. 2007). This is particularly well documented in the case of quasars, in which radio-loudness, defined to be the radio-to-optical luminosity ratio (Kellermann et al. 1989), can be monitored down to lowest values of radio luminosity associated with jet activity. (Kimball et al. 2011). However

Table 3. Results of the Kolmogorov-Smirnov test applied to the distribution in R of RL and paired RQ quasars binned according to the Eddington ratio λ_E .

$\log \lambda_E$	D	p
[-2.00, -1.55]	0.157	0.096
[-1.54, -1.39]	0.176	0.035
[-1.38, -1.23]	0.193	0.011
[-1.22, -1.11]	0.141	0.150
[-1.10, -0.99]	0.174	0.033
[-0.98, -0.88]	0.218	0.001
[-0.87, -0.70]	0.148	0.082
[-0.69, 0.11]	0.398	4.67×10^{-10}

like in X-ray BH binaries the AGN jet activity is common only at low-rate, radiatively inefficient accretion flows. At larger accretion rates, corresponding with $\lambda > 0.01$ at which accretion flows become radiatively efficient (Yuan & Narayan 2014), the jet production is typically very suppressed. This is evidenced by having only $\sim 10\%$ of quasars associated with radio sources powered by jets, and only about 2% developing luminous, extended FR II radio structures (White et al. 2007). In order to explain the existence of RL quasars and their rarity, one might consider an intermittency of jet production at high accretion rates and its low duty cycle. Such intermittency have been proposed to be driven by stochastic switches between two accretion modes, one driven by viscosity and another led by removing angular momentum via MHD outflows (Livio et al. 2003; K rding et al. 2006). However, noting the $10^7 - 10^8$ -year lifetimes of FR II radio sources (Bird et al. 2008; Antognini et al. 2012, and refs. therein), explanation for the rarity of FR II quasars in terms of the intermittent jet production scenario would require RQ quasar phase lifetimes to be longer

than the Salpeter timescale (Salpeter 1964). Furthermore, spectral properties of RQ and RL quasars are strikingly similar in all bands but radio (Sanders et al. 1989; Francis et al. 1993; Elvis et al. 1994; Zheng et al. 1997; Telfer et al. 2002; de Vries et al. 2006; Richards et al. 2006; Shang et al. 2011; Shankar et al. 2016). This suggests that production of powerful jets may not be related to some exceptional accretion mode, and seems to favour powering of jets by rotating black holes (Blandford & Znajek 1977). In such a case, the jet power scales roughly with the square of the BH spin and magnetic flux threading the BH horizon $L_j \propto a^2 \Phi_{\text{BH}}$. While value of the spin a is largely determined by cosmological evolution of BHs that involves multiple accretion and merger events (Volonteri et al. 2013), the magnetic flux Φ_{BH} is built up on black hole by advection of a poloidal magnetic field. If accumulation of the magnetic flux proceeds during the quasar phase, one might expect stronger magnetization of the accretion flows in RL quasars than in RQ quasars. Higher magnetization level of accretion flow should result in increased intensity of the hydromagnetic disc winds (Blandford & Payne 1982), both within and outside the dust sublimation radius. If we attribute the majority of AGN obscuration to dust clouds embedded in magnetized winds, the dust covering factor will be regulated by the relative power of the dusty outer wind, and the dust-free inner wind. The presence of powerful relativistic jets in RL quasars may also affect poloidal pressure balance, pushing both the dust-free inner wind and the dusty outer wind away from the jet axis.

Until now, most studies of dust covering factor were performed separately for RL and RQ quasars, and focused on their dependence on luminosity, rather than on Eddington ratio (Netzer 2015 and refs. therein). The only work to our knowledge which provides direct comparison of covering factors in RL and RQ quasars, and their dependence on Eddington ratio and BH mass, is the one by Ma & Wang (2013). No significant differences of these properties between the two quasar populations have been found. We performed a similar study, but in order to have a larger radio-loudness contrast between the RL and RQ samples, we limited the RL quasar sample only to those associated with FR II morphology that are known to be on average much radio-louder than the entire radio detected population of quasars (Lu et al. 2007). Furthermore, in order to avoid the potential effect of different black hole masses and source distances on the studied properties of RL versus RQ quasars, we compared their covering factors by including only those RQ quasars, that match the RL ones in redshift, black hole mass and Eddington ratio.

Our main results can be summarized as follows:

- Median covering factors (proxied by R) of FR II quasars and RQ quasars matched in (z ; M_{BH} ; λ_E) are comparable ($R_{50,\text{RL}} = 0.28$ and $R_{50,\text{RQ}} = 0.31$), both having very similar, fully overlapped broad distributions, with the possible exception of the highest Eddington ratios $\log \lambda_E > -0.7$;
- Dependencies of the median covering factors on the Eddington ratio, black hole mass and redshift are statistically weak. While very similar at lowest values of z , M_{BH} and λ_E , they diverge somewhat at the highest values of these parameters, with a trend of the median of R_{RL} decreasing with both λ_E and M_{BH} , and the median of R_{RQ} increasing with redshift.

Very similar covering factors of dusty obscurers in FR II and RQ quasars suggest similar accretion conditions on parsec scales. Furthermore, the lack of statistically significant dependence of covering factors (CF) on the Eddington ratio down to values $\lambda_E < 0.03$ (found also by Ma & Wang 2013) excludes the possibility that

dusty obscurers could be associated with the winds powered by radiation pressure exerted on dust. On the other hand, recent interferometric MIR observations (López-Gonzaga et al. 2016) indicate possible elongation of the dusty obscurers in the direction corresponding to the AGN polar axis (as determined by O_{III} line cones and/or jets), rather than in the equatorial plane. This would indicate outflows/winds as the loci of dust reprocessing AGN radiation into MIR. Such outflows might be powered magnetically as suggested by Emmering et al. (1992), Königl & Kartje (1994) and Elitzur & Shlosman (2006). The elongated geometry of dusty obscurers is also supported by the fact that scattering cones in quasars are much narrower than predicted by torus models (Obied et al. 2016). Significant magnetization of the accretion flows is independently supported by the fact that contribution of magnetic fields to vertical pressure in accretion discs can protect them against their gravitational fragmentation (Begelman & Pringle 2007; Salvesen et al. 2016). However, similar CF of dusty obscurers in RQ and RL quasars indicate that magnetization of accretion flows in RL quasars is not stronger than in RQ quasars. We can envisage two scenarios for reconciling this similarity with models involving the Blandford-Znajek mechanism, according to which efficiency of jet production strongly depends on the magnetic flux. They are: (1) accumulation of the magnetic flux prior to the quasar phase, which may depend strongly on the environment conditions (Sikora et al. 2013; Sikora & Begelman 2013); (2) magnetic flux accumulation during the quasar phase, in which case the amount of accumulated flux can on average be much larger in RL quasars if their lifetime is much longer than the lifetime of RQ quasars (Schawinski et al. 2015). Obviously, noting that only few nearby AGNs were imaged by MIR interferometry, it remains uncertain how representative are these objects for the entire AGN population. Noting the ambiguity of models that can successfully reproduce the observed IR spectra (Netzer 2015), better understanding of the dusty obscurer structure will need to wait for the next generation of the MIR interferometers (e.g. Lopez et al. 2014).

ACKNOWLEDGEMENTS

We thank the anonymous reviewer for helpful comments. We acknowledge financial support by the Polish National Science Centre grants 2013/09/B/ST9/00026 and 2015/18/E/ST9/00580.

REFERENCES

- Antognini, J., Bird, J., & Martini, P. 2012, *ApJ*, 756, 116
 Antonucci, R. R. J., & Miller, J. S. 1985, *ApJ*, 297, 621
 Barthel, P. D. 1989, *ApJ*, 336, 606
 Barvainis, R. 1987, *ApJ*, 320, 537
 Becker, R. H., White, R. L., & Helfand, D. J. 1995, *ApJ*, 450, 559
 Begelman, M. C., & Pringle, J. E. 2007, *MNRAS*, 375, 1070
 Bird, J., Martini, P., & Kaiser, C. 2008, *ApJ*, 676, 147
 Blandford, R. D., & Payne, D. G. 1982, *MNRAS*, 199, 883
 Blandford, R. D., & Znajek, R. L. 1977, *MNRAS*, 179, 433
 Bartscher, L., Meisenheimer, K., Tristram, K. R. W., et al. 2013, *A&A*, 558, A149
 Calderone, G., Sbarrato, T., & Ghisellini, G. 2012, *MNRAS*, 425, L41
 Chiaberge, M., Gilli, R., Lotz, J. M., & Norman, C. 2015, *ApJ*, 806, 147
 Condon, J. J., Cotton, W. D., Greisen, E. W., et al. 1998, *AJ*, 115, 1693
 de Vries, W. H., Becker, R. H., & White, R. L. 2006, *AJ*, 131, 666
 Edelson, R. A., Malkan, M. A., & Rieke, G. H. 1987, *ApJ*, 321, 233
 Elitzur, M. 2012, *ApJ*, 747, L33
 Elitzur, M., & Shlosman, I. 2006, *ApJ*, 648, L101

- Elvis, M., Wilkes, B. J., McDowell, J. C., et al. 1994, *ApJS*, 95, 1
- Emmering, R. T., Blandford, R. D., & Shlosman, I. 1992, *ApJ*, 385, 460
- Fanaroff, B. L., & Riley, J. M. 1974, *MNRAS*, 167, 31P
- Francis, P. J., Hooper, E. J., & Impey, C. D. 1993, *AJ*, 106, 417
- Hönig, S. F., Leipski, C., Antonucci, R., & Haas, M. 2011, *ApJ*, 736, 26
- Hopkins, P. F., Hayward, C. C., Narayanan, D., & Hernquist, L. 2012, *MNRAS*, 420, 320
- Kauffmann G., Heckman T. M., Best P. N., 2008, *MNRAS* 384, 953
- Kellermann, K. I., Sramek, R., Schmidt, M., Shaffer, D. B., & Green, R. 1989, *AJ*, 98, 1195
- Kimball, A. E., Kellermann, K. I., Condon, J. J., Ivezić, Ž., & Perley, R. A. 2011, *ApJ*, 739, L29
- Kishimoto, M., Hönig, S. F., Antonucci, R., et al. 2012, *Journal of Physics Conference Series*, 372, 012033
- Königl, A., & Kartje, J. F. 1994, *ApJ*, 434, 446
- Koshida, S., Minezaki, T., Yoshii, Y., et al. 2014, *ApJ*, 788, 159
- Körding, E. G., Jester, S., & Fender, R. 2006, *MNRAS*, 372, 1366
- Krolik, J. H., & Begelman, M. C. 1988, *ApJ*, 329, 702
- Lawrence, A., & Elvis, M. 2010, *ApJ*, 714, 561
- Lopez, B., Lagarde, S., Jaffe, W., et al. 2014, *The Messenger*, 157, 5
- López-Gonzaga, N., Burtscher, L., Tristram, K. R. W., Meisenheimer, K., & Schartmann, M. 2016, *A&A*, 591, A47
- Livio, M., Pringle, J. E., & King, A. R. 2003, *ApJ*, 593, 184
- Lu, Y., Wang, T., Zhou, H., & Wu, J. 2007, *AJ*, 133, 1615
- Ma, X.-C., & Wang, T.-G. 2013, *MNRAS*, 430, 3445
- Masters K. L., et al., 2010, *MNRAS*, 405, 783
- Miley, G. K., Neugebauer, G., & Soifer, B. T. 1985, *ApJ*, 293, L11
- Miller, J. S., & Goodrich, B. F. 1987, *BAAS*, 19, 695
- Netzer, H. 2015, *ARA&A*, 53, 365
- Netzer, H., Lani, C., Nordon, R., et al. 2016, *ApJ*, 819, 123
- Obied, G., Zakamska, N. L., Wylezalek, D., & Liu, G. 2016, *MNRAS*, 456, 2861
- Ramos Almeida, C., Levenson, N. A., Alonso-Herrero, A., et al. 2011, *ApJ*, 731, 92
- Rees, M. J., Silk, J. I., Werner, M. W., & Wickramasinghe, N. C. 1969, *Nature*, 223, 788
- Reyes, R., Zakamska, N. L., Strauss, M. A., et al. 2008, *AJ*, 136, 2373
- Richards, G. T., et al., 2006, *ApJS*, 166, 470
- Salpeter, E. E. 1964, *ApJ*, 140, 796
- Salvesen, G., Armitage, P. J., Simon, J. B., & Begelman, M. C. 2016, *MNRAS*, 460, 3488
- Sanders, D. B., Phinney, E. S., Neugebauer, G., Soifer, B. T., & Matthews, K. 1989, *ApJ*, 347, 29
- Schawinski, K., Koss, M., Berney, S., & Sartori, L. F. 2015, *MNRAS*, 451, 2517
- Schneider, D. P., Richards, G. T., Hall, P. B., et al. 2010, *AJ*, 139, 2360
- Shang, Z., Brotherton, M. S., Wills, B. J., et al. 2011, *ApJS*, 196, 2
- Shankar, F., Calderone, G., Knigge, C., et al. 2016, *ApJ*, 818, L1
- Shen, Y., Richards, G. T., Strauss, M. A., et al. 2011, *ApJS*, 194, 45
- Sikora, M., Stawarz, Ł., & Lasota, J.-P. 2007, *ApJ*, 658, 815
- Sikora, M., & Begelman, M. C. 2013, *ApJ*, 764, L24
- Sikora, M., Stasińska, G., Kozieł-Wierzbowska, D., Madejski, G. M., & Asari, N. V. 2013, *ApJ*, 765, 62
- Stalevski, M., Ricci, C., Ueda, Y., et al. 2016, *MNRAS*, 458, 2288
- Telfer, R. C., Zheng, W., Kriss, G. A., & Davidsen, A. F. 2002, *ApJ*, 565, 773
- van Velzen, S., Falcke, H., Körding, E. 2015, *MNRAS*, 446, 2985
- Volonteri, M., Sikora, M., Lasota, J.-P., & Merloni, A. 2013, *ApJ*, 775, 94
- White, R. L., Helfand, D. J., Becker, R. H., Glikman, E., & de Vries, W. 2007, *ApJ*, 654, 99
- Wild V., Heckman T., Charlot S., 2010, *MNRAS*, 405, 933
- Wu, X.-B., Hao, G., Jia, Z., Zhang, Y., & Peng, N. 2012, *AJ*, 144, 49
- Yuan, F., & Narayan, R. 2014, *ARA&A*, 52, 529
- Zheng, W., Kriss, G. A., Telfer, R. C., Grimes, J. P., & Davidsen, A. F. 1997, *ApJ*, 475, 469

APPENDIX A: CATALOGUE

In Table [A1](#) and [A2](#), we list the properties of our complete RL and RQ samples. The catalogues are available as supplementary material online.

This paper has been typeset from a \LaTeX file prepared by the author.

Table A1. Description of the FR II quasar sample catalogue. The catalogue is available as supplementary material online.

Column Name	Unit	Description
SDSS_Name		SDSS Name from DR7
RA_J2000	deg	Coordinates of quasars
DEC_J2000	deg	Coordinates of quasars
z		Redshift
\log_{MBH}	$\log[\text{solar mass}]$	The fiducial virial BH mass
$\log_{\text{Eddington_ratio}}$		Eddington ratio based on the fiducial virial BH mass
\log_{Lbol}	$\log W$	Bolometric luminosity
W3mag	mag	Magnitude of WISE W3 band
Flux_W3	$\text{erg s}^{-1} \text{cm}^{-2} \text{Hz}^{-1}$	Flux of WISE W3 band
\log_{v3Lv3}	$\log W$	Luminosity of WISE W3 band
LIR	$\log W$	MIR luminosity
R		Ratio of MIR luminosity to Bolometric luminosity
radio_RA	deg	R.A., geometrical centre of lobes
Radio_DE	deg	Decl., geometrical centre of lobes
lobe_flux	Jy	Total lobe flux
core_flux	Jy	Core flux (zero if no core is detected).

Table A2. Description of the RQ sample catalogue. The catalogue is available as supplementary material online.

Column Name	Unit	Description
SDSS_Name		SDSS Name from DR7
RA_J2000	deg	Coordinates of quasars
DEC_J2000	deg	Coordinates of quasars
z		Redshift
\log_{MBH}	$\log[\text{solar mass}]$	The fiducial virial BH mass
$\log_{\text{Eddington_ratio}}$		Eddington ratio based on the fiducial virial BH mass
\log_{Lbol}	$\log W$	Bolometric luminosity
W3mag	mag	Magnitude of WISE W3 band
Flux_W3	$\text{erg s}^{-1} \text{cm}^{-2} \text{Hz}^{-1}$	Flux of WISE W3 band
\log_{v3Lv3}	$\log W$	Luminosity of WISE W3 band
LIR	$\log W$	MIR luminosity
R		Ratio of MIR luminosity to Bolometric luminosity